ELSEVIER

Polymer 42 (2001) 4127–4140

polymer

www.elsevier.nl/locate/polymer

# Miscibility, crystallization kinetics and real-time small-angle X-ray scattering investigation of the semicrystalline morphology in thermosetting polymer blends of epoxy resin and poly(ethylene oxide)

Q. Guo[a,1], C. Harrats[a], G. Groeninckx[a,*], M.H.J. Koch[b]

[a]*Department of Chemistry, Laboratory of Macromolecular Structural Chemistry, Catholic University of Leuven (KU Leuven), Celestijnenlaan 200F, B-3001 Heverlee, Belgium*

[b]*European Molecular Biology Laboratory, Hamburg Outstation, EMBL c/o DESY, Notkestrasse 85, D-22603 Hamburg, Germany*

Received 31 July 2000; received in revised form 2 October 2000; accepted 22 October 2000

**Abstract**

Thermosetting polymer blends of poly(ethylene oxide) (PEO) and bisphenol-A-type epoxy resin (ER) were prepared using 4,4′-methylenebis(3-chloro-2,6-diethylaniline) (MCDEA) as curing agent. The miscibility and crystallization behavior of MCDEA-cured ER/PEO blends were investigated by differential scanning calorimetry (DSC). The existence of a single composition-dependent glass transition temperature ($T_g$) indicates that PEO is completely miscible with MCDEA-cured ER in the melt and in the amorphous state over the entire composition range. Fourier-transform infrared (FTIR) investigations indicated hydrogen-bonding interaction between the hydroxyl groups of MCDEA-cured ER and the ether oxygens of PEO in the blends, which is an important driving force for the miscibility of the blends. The average strength of the hydrogen bond in the cured ER/PEO blends is higher than in the pure MCDEA-cured ER. Crystallization kinetics of PEO from the melt is strongly influenced by the blend composition and the crystallization temperature. At high conversion, the time dependence of the relative degree of crystallinity deviated from the Avrami equation. The addition of a non-crystallizable ER component into PEO causes a depression of both the overall crystallization rate and the melting temperature. The surface free energy of folding $\sigma_e$ displays a minimum with variation of composition. The spherulitic morphology of PEO in the ER/PEO blends exhibits typical characteristics of miscible crystalline/amorphous blends, and the PEO spherulites in the blends are always completely volume-filling. Real-time small-angle X-ray scattering (SAXS) experiments reveal that the long period $L$ increases drastically with increasing ER content at the same temperatures. The amorphous cured ER component segregates interlamellarly during the crystallization process of PEO because of the low chain mobility of the cured ER. A model describing the semicrystalline morphology of MCDEA-cured ER/PEO blends is proposed based on the SAXS results. The semicrystalline morphology is a stack of crystalline lamellae; the amorphous fraction of PEO, the branched ER chains and imperfect ER network are located between PEO lamellae. © 2001 Elsevier Science Ltd. All rights reserved.

*Keywords*: Epoxy resin; Poly(ethylene oxide); Polymer miscibility; Crystallization kinetics

## 1. Introduction

Miscible blends containing a crystallizable component have attracted considerable interest. Little attention has, however, been paid to miscible or even partially miscible blends of thermosetting resins with a crystallizable linear polymer before 1989 [1–4]. From a consideration of thermodynamics, an increase in the molecular weight of either of the components of a miscible blend should reduce the entropy of mixing. Consequently, phase separation induced by cross-linking is expected for systems with a positive (endothermic) enthalpy of mixing [1]. Miscibility and hydrogen bonding interactions between the components have, however, recently been observed in a few cases, even for some highly cross-linked blends [5–10]. The hydrogen-bonding interaction was considered to be the driving force for the miscibility, and it is responsible for the favorable exothermic heat of mixing that is the thermodynamic basis of the miscibility in these thermosetting polymer blends.

Crystallization in thermosetting polymer blends containing a crystallizable thermoplastic component will actually be greatly affected by both the miscibility and phase behavior of the crosslinked blends and the topological effect of the network. The crystallization kinetics and semicrystalline morphology in miscible thermosetting polymer blends

* Corresponding author. Tel.: +32-16-32-74-40; fax: +32-16-32-74-90.

[1] On leave from Department of Polymer Science and Engineering, University of Science and Technology of China, Hefei, China.

0032-3861/01/$ - see front matter © 2001 Elsevier Science Ltd. All rights reserved.
PII: S0032-3861(00)00813-2

containing one crystallizable component have hitherto received relatively little attention. In such systems, curing results in chain extension, branching, crosslinking and significant changes in chemical and physical properties of the non-crystallizable component. This may influence the chain mobility and the free energy of nucleation, and hence have dramatic influence on the crystallization of the crystallizable component. It is however rather difficult to image the segregation process of a crosslinked, thermosetting polymer in the blend during the crystallization process of the crystallizable component. The topological influence of the network of crosslinked component on the crystallization and segregation should be considerable. It is therefore important to investigate the semicrystalline morphology and lamellar structure of this type of thermosetting polymer blends.

Thermosetting polymer blends of poly(ethylene oxide) (PEO) with several cured epoxy resins have been examined previously [9–12]. It was shown that the miscibility of an epoxy resin with a linear polymer is very dependent on the nature of curing agent. Below we present results of an investigation on a completely miscible thermosetting polymer blend of PEO and bisphenol-A-type epoxy resin (ER) cured with 4,4′-methylenebis(3-chloro-2,6-diethylaniline) (MCDEA). Miscibility, thermal properties and isothermal crystallization kinetics of the MCDEA-cured ER/PEO blends are studied using differential scanning calorimetry (DSC). Fourier-transform infrared (FTIR) spectroscopy is used to study the hydrogen-bonding interaction between the components. Real-time small-angle X-ray scattering (SAXS) experiments have been performed to investigate the semicrystalline morphology, which provides important information on the crystalline lamellar structure of PEO and segregation of the amorphous MCDEA-cured ER component in this type of blends. On the basis of the SAXS results, a model describing the semicrystalline morphology and lamellar structure of MCDEA-cured ER/PEO blends is proposed.

## 2. Experimental

### 2.1. Materials and sample preparation

Poly(ethylene oxide) with a viscosity-average molecular weight of 17,000 and a polydispersity of 1.35 was obtained from Janssen Chemical Company, Belgium. The uncured epoxy resin is diglycidyl ether of bisphenol A (DGEBA) (Epikote 828EL, Shell Company, Netherlands) and has an epoxide equivalent weight of 190. Prior to use, it was degassed under vacuum at 120°C for at least 24 h to remove any volatile impurities. 4,4′-methylenebis(3-chloro-2,6-diethylaniline) (MCDEA) (Aldrich Company, Inc., USA) was used as curing agent.

To prepare the MCDEA-cured ER/PEO blends, PEO was first dissolved in ER by continuous stirring at 90°C. The curing agent MCDEA was then added to the mixture by continuous stirring until a homogeneous ternary mixture was obtained. The amount of MCDEA used in the mixtures was 50 wt% relative to the content of DGEBA, i.e. with MCDEA/DGEBA = 50/100 (w/w) in the mixtures, which is approximately in stoichiometric epoxide/amine ratios. The samples of ternary mixture were cured successively at 130°C for 2 h, 150°C for 2 h and 170°C for 2 h.

### 2.2. Differential scanning calorimetry (DSC)

The calorimetric measurements were made on a Perkin–Elmer DSC-7 differential scanning calorimeter in a dry nitrogen atmosphere. Indium and tin standards were used for calibration for low and high temperature regions, respectively. The sample weight used in the DSC pan was about 8 mg. All samples were first heated to 100°C at a rate of 20°C/min (first heating scan) and kept at that temperature for 2 min; subsequently they were cooled at a rate of −20°C/min to detect crystallization (cooling scan). Following the cooling scan, a second scan was conducted at the same heating rate as the first. The midpoint of the slope change of the heat capacity plot of the second heating scan was taken as the glass transition temperature ($T_g$). The crystallization temperature ($T_c$) was taken as the minimum of the exothermic peak, whereas the melting temperature ($T_m$) was taken as the maximum of the endothermic peak. The heat of fusion ($\Delta H_f$) and the heat of crystallization ($\Delta H_c$) were evaluated from the areas of the melting and crystallization peaks, respectively.

For the study of isothermal crystallization, the samples were first heated to 100°C and maintained at this temperature for 5 min to erase their thermal histories. They were then cooled to the appropriate crystallization temperature, $T_c$, at a rate of 100°C/min. The heat generated during the development of the crystalline phase was recorded up to a vanishing thermal effect and analyzed according to the usual procedure to evaluate the relative degree of crystallinity, $X_t$

$$X_t = \frac{\int_{t_0}^{t} \left(\frac{\partial H}{\partial t}\right)_{T,P} dt}{\int_{t_0}^{\infty} \left(\frac{\partial H}{\partial t}\right)_{T,P} dt} \quad (1)$$

where $t_0$ is the time at which the sample reaches isothermal conditions, as indicated by a flat base line after an initial spike in the thermal curve.

To study the melting behavior, the isothermally crystallized samples were subsequently reheated to 80°C at a rate of 20°C/min. The position of the maximum of the endothermic peak was taken as the melting temperature, $T_m$.

### 2.3. Fourier-transform infrared (FTIR) spectroscopy

FTIR measurements were made with a Perkin–Elmer 2000 Fourier-transform infrared spectrometer for the

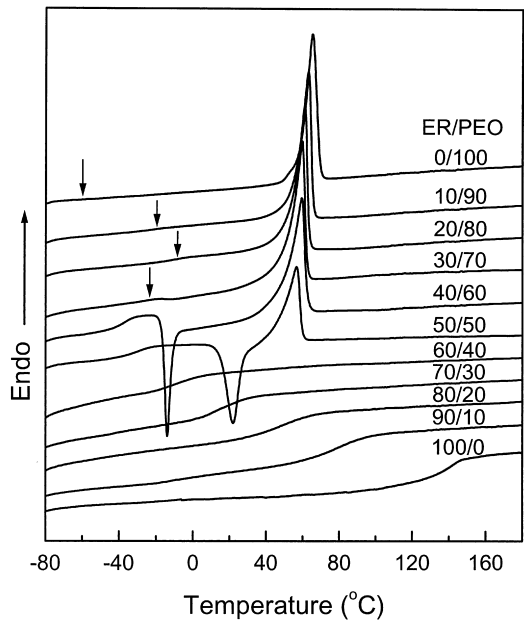


Fig. 1. DSC thermograms of the second scan of the MCDEA-cured ER/PEO blends after the cooling scan. The heating rate is 20°C/min.

cured ER/PEO blends. Little lumps scraped from the cured samples were mixed with KBr in a mortar and then grounded into fine powder, which was further pressed into thin sheets for FTIR measurements. All spectra were recorded at room temperature and signal-averaged over 64 scans at a resolution of 2 $cm^{-1}$.

### 2.4. Morphological observations

The overall morphology of the pure PEO, the ER/PEO blends, as well as the MCDEA-cured ER/PEO blends was investigated by optical microscopy using an Olympus BH2 apparatus equipped with cross-polarizers. The samples between two glass covers were crystallized from the melt before observation.

### 2.5. Real-time SAXS measurements

Time-resolved SAXS measurements were carried out on the double focusing monochromator-mirror camera X33 [13] of the EMBL in HASYLAB on the storage ring DORIS III of the Deutsches Electronen Synchrotron (DESY) in Hamburg using a wavelength of 0.15 nm. Samples about 1 mm thick were sealed between thin (70 μm) aluminum foils and placed in a Mettler FP-82 hot stage mounted in the X-ray beam path. During these experiments, the specimens were first kept at 80°C for 1 min and then cooled at 10°C/min to 20°C; they were kept at 20°C for 15 seconds, followed by heating to 80°C at 10°C/min. The SAXS patterns were collected every 15 seconds, corresponding to a temperature increment of 2.5°C. The data were processed using the OTOKO software package [14]. The original SAXS data were smoothed and corrected for background scattering by the subtraction of an amorphous sample in the molten state.

## 3. Results and discussion

### 3.1. Miscibility and thermal properties

The MCDEA-cured ER/PEO blends with 30 wt% or higher PEO were opaque at room temperature; this resulted from the crystallization of PEO in the blends. All the blends were however transparent just above the melting point of PEO, indicating that PEO and the cured ER are miscible in the molten state. The DSC thermograms of the second scan of the MCDEA-cured ER/PEO blends are shown in Fig. 1 and the results are summarized in Table 1 and Fig. 2. The degree of crystallinity, $X_c$, was calculated by the following equations:

$$X_c(\text{blend}) = (\Delta H_f + \Delta H_c)/\Delta H^\circ_f \quad (2)$$

$$X_c(\text{PEO}) = X_c(\text{blend})/W(\text{PEO}) \quad (3)$$

where $\Delta H^\circ_f = 205$ J/g is the heat of fusion of 100% crystalline PEO [15], $\Delta H_f$ is the heat of fusion of the

Table 1
Thermal properties from the second scans of MCDEA-cured ER/PEO blends

| ER/PEO | $T_g$ (°C) | $T_m$ (°C) | $\Delta H_f$ (J/g blend) | $T_c$ (°C) | $\Delta H_c$ (J/g blend) | $X_c$(blend) (%) | $X_c$(PEO) (%) |
|---|---|---|---|---|---|---|---|
| 0/100 | −62 | 65 | 166.2 | | | 81.1 | 81.1 |
| 10/90 | −25 | 63 | 139.8 | | | 68.2 | 75.8 |
| 20/80 | −14 | 61 | 122.0 | | | 59.5 | 74.4 |
| 30/70 | −28 | 60 | 105.5 | | | 51.5 | 73.5 |
| 40/60 | −37 | 59 | 82.6 | −14 | −66.5 | 7.9 | 13.2 |
| 50/50 | −28 | 57 | 58.9 | 22 | −52.6 | 3.1 | 6.2 |
| 60/40 | −9 | | | | | | |
| 70/30 | 18 | | | | | | |
| 80/20 | 49 | | | | | | |
| 90/10 | 80 | | | | | | |
| 100/0 | 138 | | | | | | |

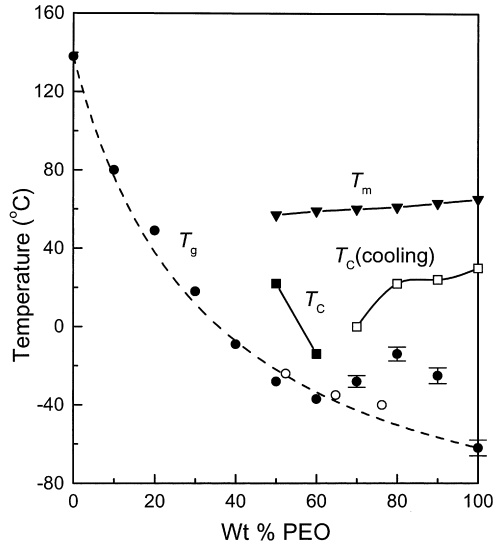


Fig. 2. Thermal properties of the second scan of the MCDEA-cured ER/PEO blends. (●) Experimental plot of $T_g$ vs. overall blend composition, (○) plot of $T_g$ vs. calculated amorphous composition, and (– – – –) theoretical curve of $T_g$ vs. composition as predicted by the Gordon–Taylor equation using a $k$ value of 0.25. The $T_c$(cooling) (□) as a function of composition is also given.

blend and $\Delta H_c$ is the heat of crystallization during the same heating scan.

As illustrated in Fig. 1, the blends display a single, composition dependent $T_g$, strongly indicating that the two components are miscible in the amorphous state. The $T_g$ value of the blends as a function of their composition is given in Fig. 2 (full circles). The $T_g$-composition dependence can be described using the Gordon–Taylor equation [16]

$$T_g(\text{blend}) = (W(\text{PEO})T_g(\text{PEO}) + kW(\text{ER})T_g(\text{ER}))/(W(\text{PEO}) + kW(\text{ER})) \quad (4)$$

where $T_g$(blend) is the glass transition temperature of the blend, $T_g$(ER) and $T_g$(PEO) are the $T_g$'s of plain ER and PEO, respectively, W(ER) and W(PEO) represent the weight fractions of ER and PEO, respectively, and k is a constant. The broken curve in Fig. 2 is drawn using a $k$-value of 0.25.

Fig. 2 illustrates that for the ER/PEO blends with 70 wt% or more PEO, the values of $T_g$ display a positive deviation from those predicted by the Gordon–Taylor equation, which is considered to be the result of the high crystallinity of PEO. Because of the crystallization of PEO in these blend compositions, the weight fraction of PEO in the amorphous phase, W'(PEO), is not equal to the overall weight fraction of PEO in the blend, W(PEO). These quantities are related as follows [17]:

$$W'(\text{PEO}) = (W(\text{PEO}) - X_c(\text{blend}))/(1 - X_c(\text{blend})) \quad (5)$$

A replot of $T_g$ values (open circles) vs. the weight fraction of PEO in the amorphous phase, calculated using Eq. (5), fits the Gordon–Taylor equation quite well. However, the reduction in $T_g$ of the cured blends can result from a combination of two plasticization effects: internal and external. The dilution effect of the PEO component can result in a reduction in crosslinking density of the network and hence a reduction in its $T_g$. The crosslinking density of the ER network decreases with increasing content of PEO. For the blends with low PEO content, a three-dimensional crosslinking network structure forms. In contrast, for the blends with low ER content, only an imperfect network is formed and there are highly branched ER chain molecules.

Fig. 2 also contains the $T_c$ and $T_m$ values from the second scans as a function of the blend composition. Neither a crystallization exotherm nor a melting endotherm is observed in the blends with 60 wt% or more ER, indicating that PEO in these blends exhibits no tendency to crystallize during the cooling scan and the subsequent second heating scan. For the blends containing 70 wt% PEO or more, no crystallization exotherm is observed during heating since the crystallization of PEO was sufficiently rapid to occur completely during the cooling scan. In contrast, the blends with 50–60 wt% PEO show a crystallization exotherm during heating above their $T_g$; their $T_c$ increases with increasing ER content, indicating a progressively more difficult crystallization of PEO in these blends.

The crystallization rate of PEO in the cured ER/PEO blends also decreases during cooling from the melt. Fig. 3 shows DSC thermograms of the cooling scan for the cured ER/PEO blends at a cooling rate of 20°C/min from 100°C.

The crystallization peak shifts to lower temperatures with

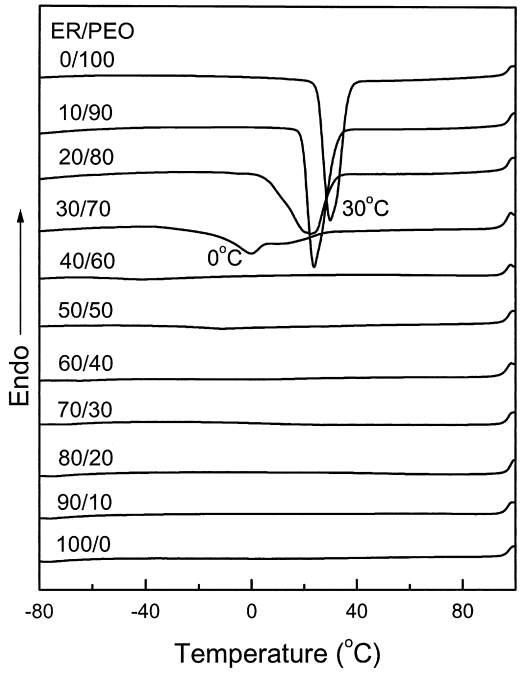


Fig. 3. Crystallization curves of the MCDEA-cured ER/PEO blends during the cooling at −20°C/min.

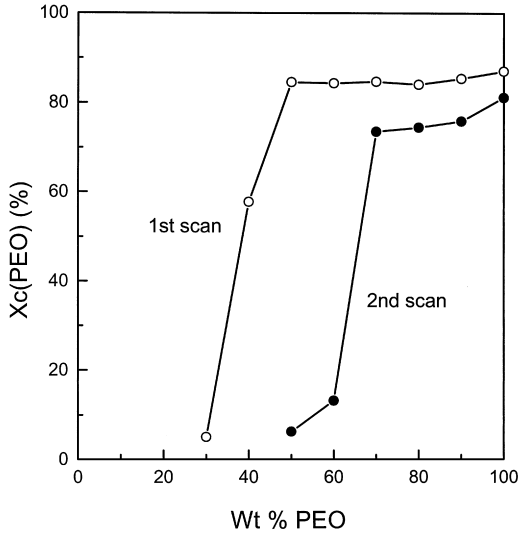


Fig. 4. $X_c$(PEO) vs. PEO weight fraction of the MCDEA-cured ER/PEO blends. (○) First scan; (●) second scan.

increasing ER content, and there is no crystallization exotherm during the cooling run for the blends containing less than 70 wt% PEO. The crystallization temperature during the cooling scan, $T_c$(cooling), is also plotted in Fig. 2 as a function of composition. The values of $T_c$(cooling) decrease rapidly with increasing ER content. The overall crystallization rate of PEO in the cured blends decreases rapidly with increasing ER content, which can be ascribed to the much higher $T_g$ of the MCDEA-cured ER (138°C) compared to that of PEO (−62°C). Fig. 3 illustrates that the 30/70 ER/PEO blend displays a crystallization exotherm at 0°C with a large shoulder on the high temperature side. It is known that PEO can crystallize by either heterogeneous or homogeneous nucleation [18]. The shape of the crystallization exotherm of the 30/70 ER/PEO blend can be attributed to sequential heterogeneous and homogeneous nucleation. Initially, crystallization is induced by heterogeneous nucleation starting from 28°C during the cooling scans. The crystallization rate of PEO in the 30/70 ER/PEO blend is very slow and the number of heterogeneous nuclei is small. Consequently, the crystallization process is not completed when the temperature reaches about 5°C where homogeneous nucleation starts after formation of primary nuclei by the PEO chains.

Fig. 2 also illustrates that the $T_m$ of PEO in the blends substantially decreases with increasing ER content. The $T_m$-depression is a common phenomenon for miscible blends containing one crystallizable component [19–21]. Morphological factors can also influence on the $T_m$ of PEO.

The values of $X_c$(PEO) for the ER/PEO blends are plotted as a function of blend composition in Fig. 4. The $X_c$(PEO) values for the first scan of the as-prepared samples are all higher than those for the second scan. For the second scan, $X_c$(PEO) decreases only slightly with PEO content down to 70 wt% and then rapidly at lower PEO contents. For the first scan of the as-prepared samples, $X_c$(PEO) remains almost unchanged for PEO contents between 100 and 50 wt% PEO. The crystallization of the as-prepared samples is much more complete than that of the second scan because of the long residence time at room temperature.

### 3.2. Hydrogen-bonding interactions

PEO has been shown to be miscible with many other polymers due to its high potentiality to form hydrogen bonds with these polymers. In particular it is miscible with poly(hydroxyether of bisphenol A) (phenoxy) [22], and it has been shown that there is hydrogen bonding interaction between PEO and phenoxy [23]. Bisphenol A-type epoxy resin has a structure similar to phenoxy which can be considered as a linear model bisphenol A-type epoxy resin (i.e. a linear high-molecular-weight polymer of bisphenol A-type epoxy resin).

Although the ER sample used had a low hydroxyl content, the curing reaction between epoxy and amine groups will result in the formation of hydroxyl groups in the MCDEA-cured ER molecules. These can form many hydrogen bonds with the ether oxygens of PEO. FTIR studies reveals that hydrogen bonding in the cured blends occurs between the hydroxyl groups of MCDEA-cured ER and the ether oxygens of PEO.

Fig. 5 shows the FTIR spectra of the MCDEA-cured ER/PEO blends in the stretching region of the ER hydroxyl groups ranging between 3000 and 3800 $cm^{-1}$. The spectrum of the pure MCDEA-cured ER in this region has two components. A broad band centered at 3417 $cm^{-1}$ is attributed to the self-associated hydroxyl (i.e. hydrogen bonded

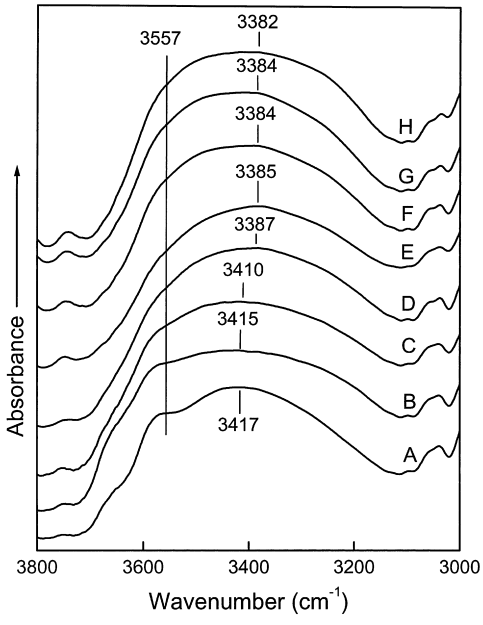


Fig. 5. FTIR spectra of the MCDEA-cured ER/PEO blends in the 3000–3800 $cm^{-1}$ region. ER/PEO: (A) 100/0; (B) 90/10; (C) 80/20; (D) 70/30; (E) 60/40; (F) 50/50; (G) 40/60; and (H) 30/70.

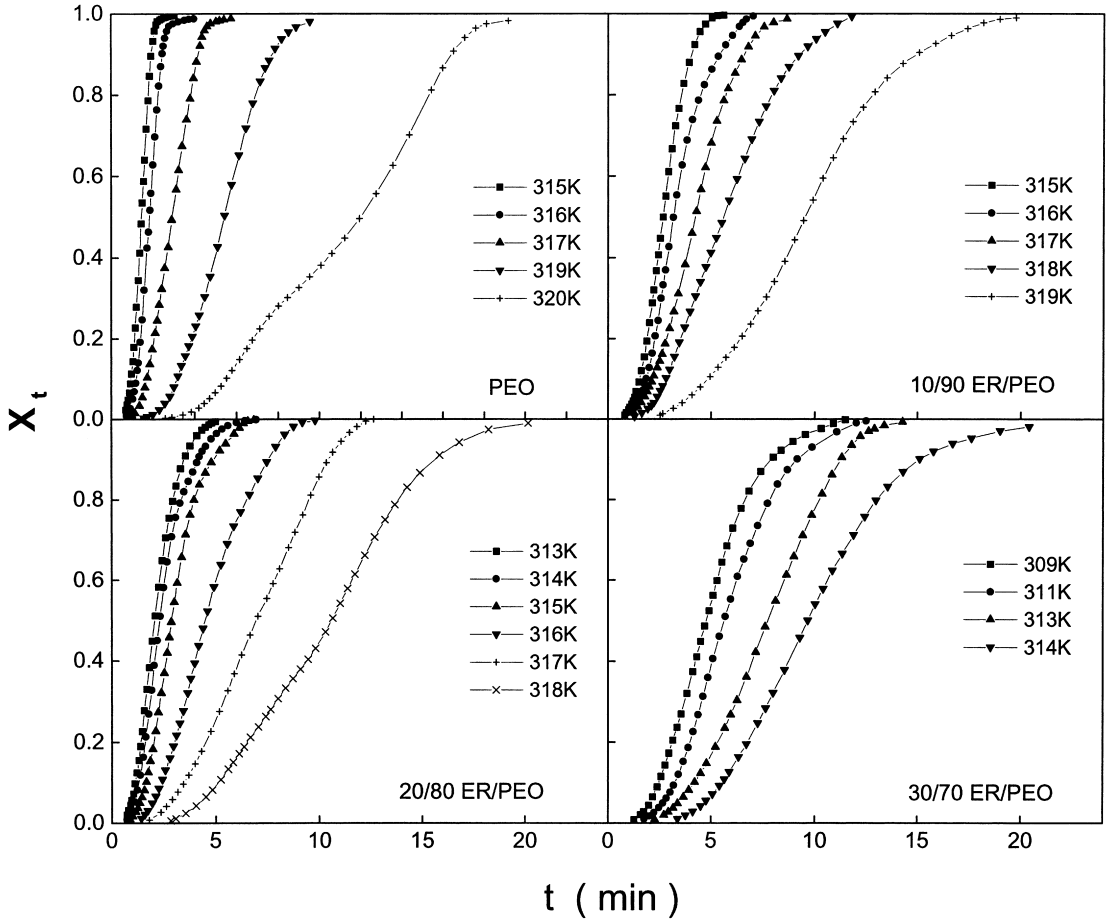


Fig. 6. Development of the relative degree of crystallinity with time for isothermal crystallization of MCDEA-cured ER/PEO blends. The figures indicate the respective crystallization temperatures in K.

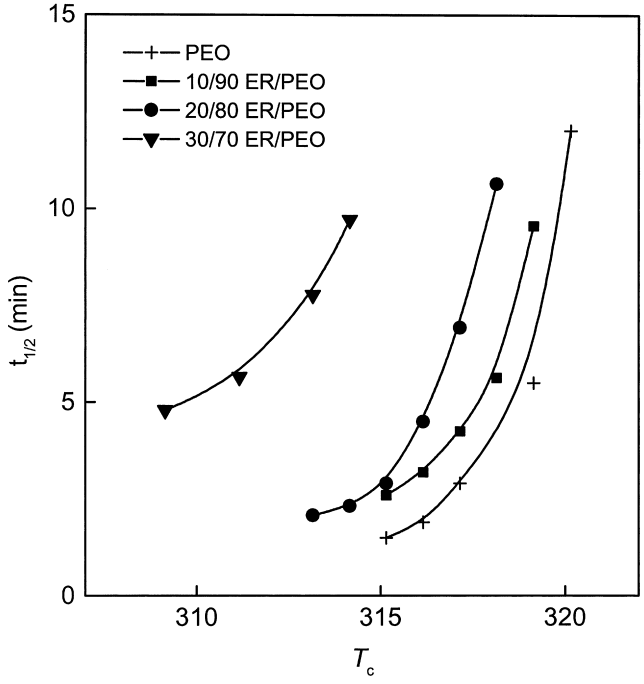


Fig. 7. Half-time of crystallization $t_{1/2}$ as a function of crystallization temperature $T_c$.

hydroxyl groups) and a relatively sharp band at 3557 $cm^{-1}$ is assigned to non-associated, free hydroxyl groups. Upon blending with PEO, the non-associated hydroxyl band at 3557 $cm^{-1}$ does not shift in the blend. In contrast, the associated hydroxyl band at 3417 $cm^{-1}$ shifts to lower frequencies with increasing PEO concentration, indicating that there is hydrogen bonding between the hydroxyl groups of ER and the ether oxygens of PEO. The ratio of intensity between the hydrogen bonded hydroxyl band and the free hydroxyl band increases with increasing PEO concentration, indicating the gradual increase of the relative percentage of hydrogen bonded hydroxyls in the blends. The frequency difference between the free hydroxyl absorption and that of the hydrogen bonding species ($\Delta\nu$) is a measure of the average strength of the intermolecular interactions [24]. The above results thus indicate that the average strength of the hydrogen bond between the hydroxyl groups of ER and the ether oxygens of PEO in the cured blends ($\Delta\nu = 175\ cm^{-1}$ for the cured 30/70 ER/PEO blend) is higher than that between the hydroxyl groups in the pure cured ER ($\Delta\nu = 140\ cm^{-1}$). Coleman and Moskala found that the average strength of the hydrogen bond between the PEO ether oxygen and the phenoxy

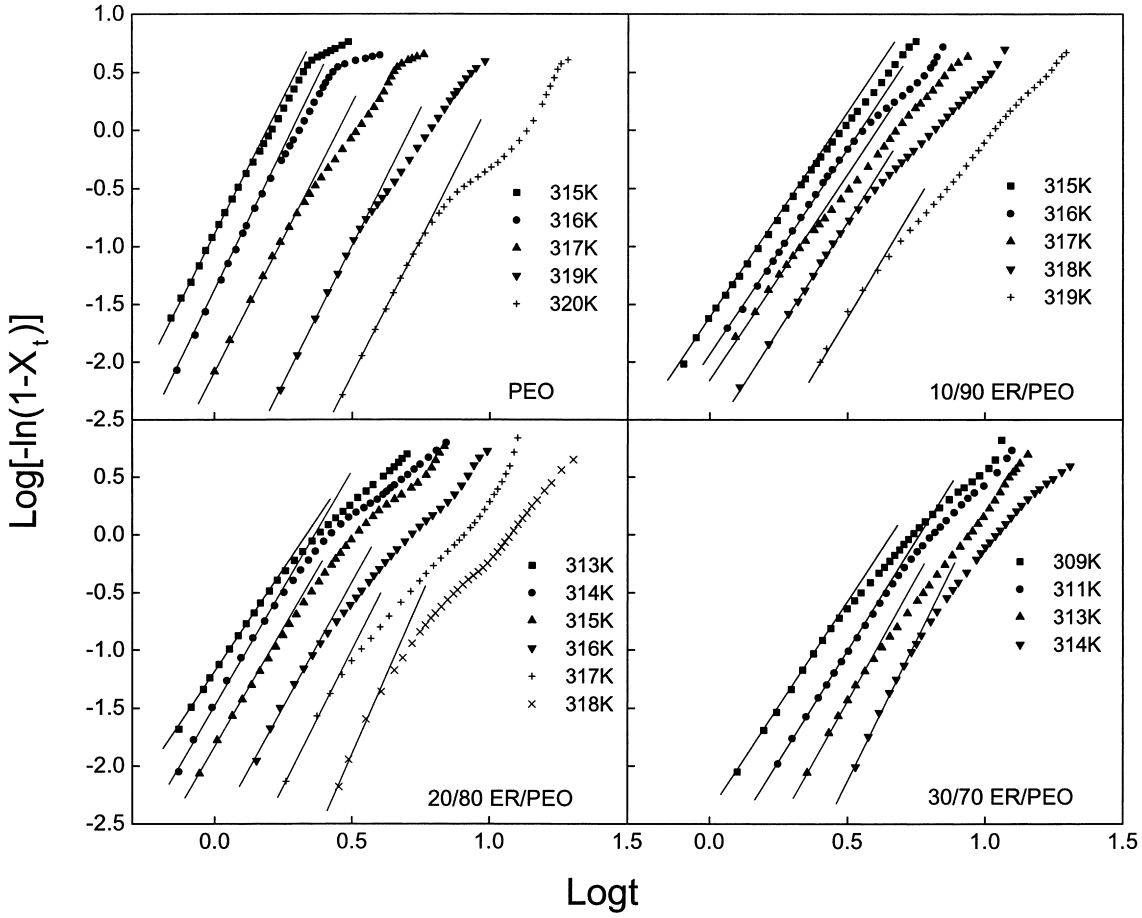


Fig. 8. Plots of $\log[-\ln(1 - X_t)]$ vs. $\log t$ for isothermal crystallization of MCDEA-cured ER/PEO blends. The figures indicate the respective crystallization temperatures in K.

Table 2
Values of the overall kinetic rate constant $K_n$, the Avrami index $n$ and the melting temperature $T_m'$ at various crystallization temperature, $T_c$

| | $T_c$ (K) | $T_m'$ (K) | $K_n$ ($min^{-n}$) | $n$ |
|---|---|---|---|---|
| Pure PEO | 315 | 339.6 | $1.24 \times 10^{-1}$ | 4.6 |
| | 316 | 334.0 | $4.09 \times 10^{-2}$ | 4.9 |
| | 317 | 340.1 | $8.14 \times 10^{-3}$ | 4.7 |
| | 319 | 340.5 | $3.97 \times 10^{-4}$ | 4.8 |
| | 320 | 340.8 | $3.19 \times 10^{-5}$ | 4.6 |
| 10/90 ER/PEO | 315 | 338.0 | $2.48 \times 10^{-2}$ | 3.5 |
| | 316 | 338.1 | $1.18 \times 10^{-2}$ | 3.5 |
| | 317 | 338.4 | $7.09 \times 10^{-3}$ | 3.6 |
| | 318 | 338.6 | $2.22 \times 10^{-3}$ | 3.7 |
| | 319 | 338.9 | $2.58 \times 10^{-4}$ | 4.0 |
| 20/80 ER/PEO | 313 | 338.1 | $6.67 \times 10^{-2}$ | 3.5 |
| | 314 | 338.4 | $3.38 \times 10^{-2}$ | 4.1 |
| | 315 | 338.4 | $1.48 \times 10^{-2}$ | 4.1 |
| | 316 | 338.7 | $2.84 \times 10^{-3}$ | 4.3 |
| | 317 | 339.0 | $4.57 \times 10^{-4}$ | 4.7 |
| | 318 | 339.1 | $2.70 \times 10^{-5}$ | 5.4 |
| 30/70 ER/PEO | 309 | 336.7 | $3.96 \times 10^{-3}$ | 3.7 |
| | 311 | 336.9 | $1.24 \times 10^{-3}$ | 3.8 |
| | 313 | 337.3 | $2.76 \times 10^{-4}$ | 4.2 |
| | 314 | 337.5 | $3.04 \times 10^{-5}$ | 4.8 |

hydroxyl group ($\Delta\nu = 270\ cm^{-1}$ for 50/50 phenoxy/PEO blend) in phenoxy/PEO system is also higher than that between the hydroxyl groups in plain phenoxy ($\Delta\nu = 160\ cm^{-1}$) [23].

The analysis of the FTIR spectra suggests that hydrogen-bonding interaction is an important driving force for the miscibility of the ER/PEO blends. This further confirms that the MCDEA-cured ER/PEO blends are completely miscible.

### 3.3. Isothermal crystallization kinetics

*Overall crystallization rate.* Typical crystallization isotherms, obtained by plotting $X_t$ against time $t$, are reported in Fig. 6 for PEO and MCDEA-cured ER/PEO blends. The crystallization isotherms are sigmoidal. The isotherm curves shift to the right along the time axis with increasing $T_c$ and the slope of all isotherms decreases with increasing $T_c$, indicating progressively slower crystallization rates. In the present experimental conditions, nucleation is thus the dominant factor, determining the overall crystallization rate. The half-time of crystallization, $t_{1/2}$, defined as the time required for the development of half of the final

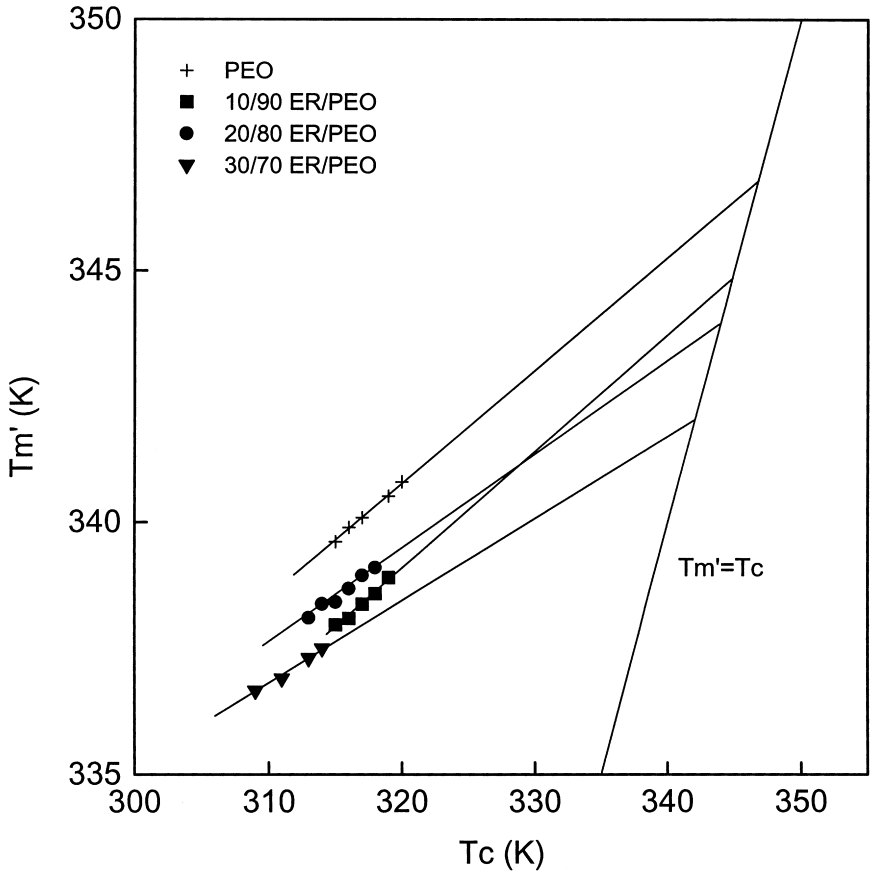


Fig. 9. Plots of the observed melting temperature $T_m'$ vs. $T_c$ for MCDEA-cured ER/PEO blends.

crystallinity was evaluated from these curves. The $t_{1/2}$ values are plotted against $T_c$ for pure PEO and for the blends in Fig. 7 which illustrates that (i) Incorporation of non-crystallizable cured ER component into PEO depresses the overall crystallization rate of PEO and (ii) at constant $T_c$, the overall crystallization rate decreases significantly with increasing concentration of the non-crystallizable ER component.

The kinetics of the isothermal crystallization from the melt of the ER/PEO blends was analyzed on the basis of the Avrami equation [25]:

$$\log[-\ln(1 - X_t)] = \log K_n + n \log t \quad (6)$$

where $K_n$ is the overall kinetic rate constant, and $n$ the Avrami index which depends on the nucleation and growth mechanism of the crystals [26].

Plots of $\log[-\ln(1 - X_t)]$ vs. $\log t$ for PEO and the blends are shown in Fig. 8. The experimental data are fitted by the Avrami equation only for the early part of transformation. The time dependence of the relative degree of crystallinity at high conversion deviates from the Avrami equation. A similar deviation from the Avrami equation has been reported by Ong and Price for poly(ϵ-caprolactone)/poly(vinyl chloride) blends [27]. Wunderlich also showed that the Avrami equation is usually only valid at low conversion [28].

In order to evaluate $K_n$ and $n$, only the experimental data at low conversion were used. The values of $K_n$ and $n$ determined by the intercepts and slopes, respectively, of the straight lines in Fig. 8 are listed in Table 2.

In almost all cases, the values of n are nonintegral, in contrast with the theoretical prediction. Nonintegral values are generally accounted for by mixed growth and/or surface nucleation and two-stage crystallization. Grenier and Prud'homme [29] have shown that experimental factors such as an erroneous determination of the "zero" time or of the melting enthalpy of the polymer at a given time can cause n to be nonintegral. The $n$-values obtained are between 3.5 and 5.4, they do not change much with ER concentration in the ER/PEO blends. This fact indicates that the incorporation of cured ER does not significantly influence the mechanism of nucleation and growth of the PEO under the experimental conditions used.

*Melting behavior and equilibrium melting points.* The maximum of the re-melting DSC curve was considered to correspond to the melting temperature, $T_m'$, for different crystallization temperatures, $T_c$. Table 2 also presents the observed melting temperature, $T_m$, for the pure PEO as well as for the MCDEA-cured ER/PEO blends.

The plots of $T_m'$ vs. $T_c$ in Fig. 9 illustrate that linear dependence of $T_m'$ on $T_c$ in the range of $T_c$ examined. The experimental data can be fitted by the Hoffman–Weeks

Table 3
Values of the equilibrium melting temperature $T_m^{eq}$, the stability parameter $\phi$, the nucleation factor $K_g$, the surface free energy of folding $\sigma_e$, and the pre-exponential factor $A_0$

| | $T_m^{eq}$ (K) | $\phi$ | $K_g$ (K$^2$) | $\sigma_e$ (J/m$^2$) | $A_0$ |
|---|---|---|---|---|---|
| Pure PEO | 346.8 | 0.225 | $1.36\times10^5$ | $6.25\times10^{-2}$ | $6.62\times10^{11}$ |
| 10/90 ER/PEO | 344.9 | 0.234 | $8.14\times10^4$ | $3.76\times10^{-2}$ | $4.33\times10^{13}$ |
| 20/80 ER/PEO | 344.0 | 0.189 | $7.42\times10^4$ | $3.44\times10^{-2}$ | $1.77\times10^{12}$ |
| 30/70 ER/PEO | 342.0 | 0.161 | $1.14\times10^5$ | $5.32\times10^{-2}$ | $1.72\times10^{11}$ |

equation [30,31]

$$T'_m = \phi T_c + (1-\phi)T_m^{eq} \quad (7)$$

where $T_m^{eq}$ is the equilibrium melting point, $\phi = 1/\gamma$ is the stability parameter which depends on the crystal thickness, whereas $\gamma$ is the ratio of the lamellar thickness $\lambda$ to the lamellar thickness of the critical nucleus $\lambda^*$ at $T_c$. In Eq. (7), $\phi$ may assume values between 0 and 1. $\phi = 0$ implies $T'_m = T_m{}^{eq}$, whereas $\phi = 1$ implies $T'_m = T_c$. Consequently, the crystals are most stable for $\phi = 0$ and are inherently unstable for $\phi = 1$.

As shown in Fig. 9, the values of $T_m^{eq}$ can be evaluated by extrapolating the least-squares fit lines of the experimental data according to Eq. (7) to intersect the line of $T'_m = T_c$. The $\phi$ parameters can be determined from the slope of these fit lines. Both, the values of $T_m^{eq}$ and of $\phi$ for all compositions are listed in Table 3. There is obviously a depression of $T_m^{eq}$ for the blends and its magnitude increases with increasing amorphous ER content. In Table 3, the values of the stability parameter $\phi$ range from 0.161 to 0.234, suggesting that the crystals are fairly stable.

*Temperature dependence of $K_n$.* The kinetic theory of polymer crystallization developed by Hoffman et al. [32–34] has been generally employed to analyze experimental crystallization data concerning the spherulite growth rate. According to this theory, the dependence of the growth rate G on the crystallization temperature, $T_c$, and the undercooling, $\Delta T = T_m^{eq} - T_c$, is described by the following equation:

$$G = v_2 G_0 \exp\left(\frac{-\Delta F^*}{RT_c}\right)\exp\left(\frac{-\Delta\Phi^*}{k_B T_c}\right) \quad (8)$$

where $G_0$ is a preexponential factor, generally assumed to be constant or proportional to $T_c$, $\Delta F^*$ the activation energy for the transport of the crystallizing units across the liquid–solid interface, $\Delta\Phi^*$ the free energy required to form a nucleus of critical size. R is the gas constant and $k_B$ the Boltzman constant whereas $v_2$ the PEO volume fraction.

According to Boon and Azcue [35], $\Delta\Phi^*$ in Eq. (4) can be expressed as

$$\frac{\Delta\Phi^*}{k_B T_c} = \frac{K_g}{fT_c\Delta T} + \frac{2\sigma T_m^{eq}\ln v_2}{b_0\Delta H_f\Delta T} \quad (9)$$

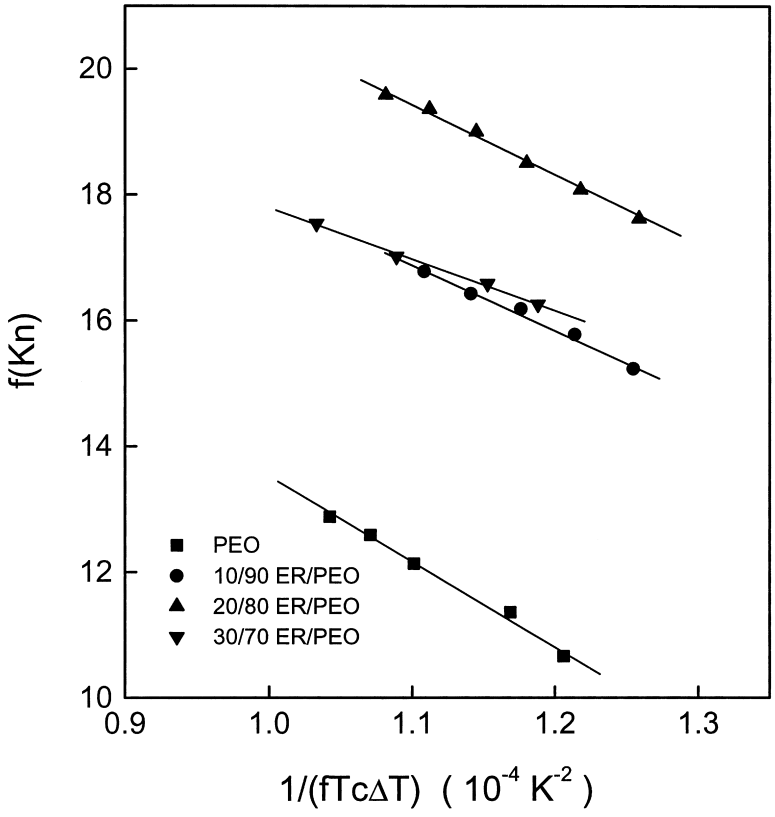


Fig. 10. Plots of the quantity $f(K_n)$ vs. $1/(fT_c\Delta T)$ for MCDEA-cured ER/PEO blends.

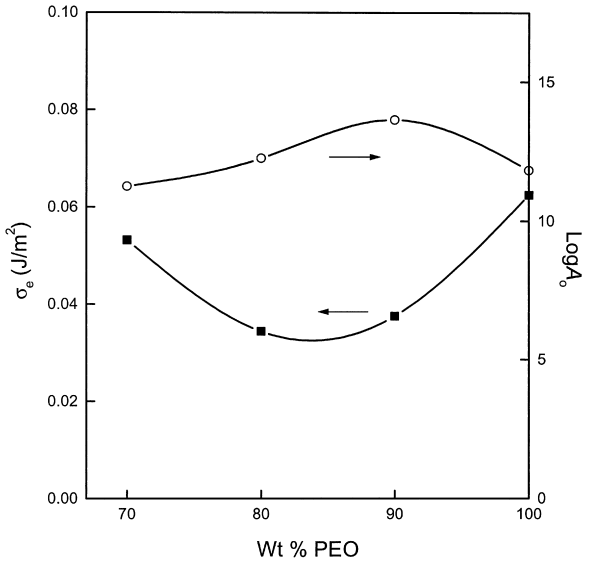


Fig. 11. Plots of $\sigma_e$ (■) and $\log A_0$ (○) vs. the weight fraction of PEO for MCDEA-cured ER/PEO blends.

$$K_g = \frac{Zb_0\sigma\sigma_e T_m^{eq}}{k_B \Delta H_f} \tag{10}$$

$$f = \frac{2T_c}{T_m^{eq} + T_c} \tag{11}$$

where $K_g$ is the nucleation factor, $f$ the correction factor for the heat of fusion; $\sigma$ and $\sigma_e$ the interfacial free energies of the unit area parallel and perpendicular, respectively, to the molecular chain axis, $b_0$ the distance between two adjacent fold planes, $\Delta H_f$ the enthalpy of fusion per unit volume of the crystalline component, and $Z$ a coefficient that depends on the growth regime: $Z = 4$ in Regimes I and III, and $Z = 2$ in Regime II [36].

The $\Delta F^*$ in Eq. (8) can be estimated with a satisfactory precision using the WLF equation [37]

$$\Delta F^* = \frac{C_1 T_c}{C_2 + T_c - T_g} \tag{12}$$

where $_{C1}$ and $C_2$ are constants (generally assumed to be 4120 cal/mol and 51.6 K, respectively) and $T_g$ is the glass transition temperature.

For the overall crystallization rate, we used $G = CK_n^{1/n}$ where $C$ is a constant. Assuming [38] that $\sigma = 0.1 b_0 \Delta H_f$ and taking into account relations (8), (9) and (12), the

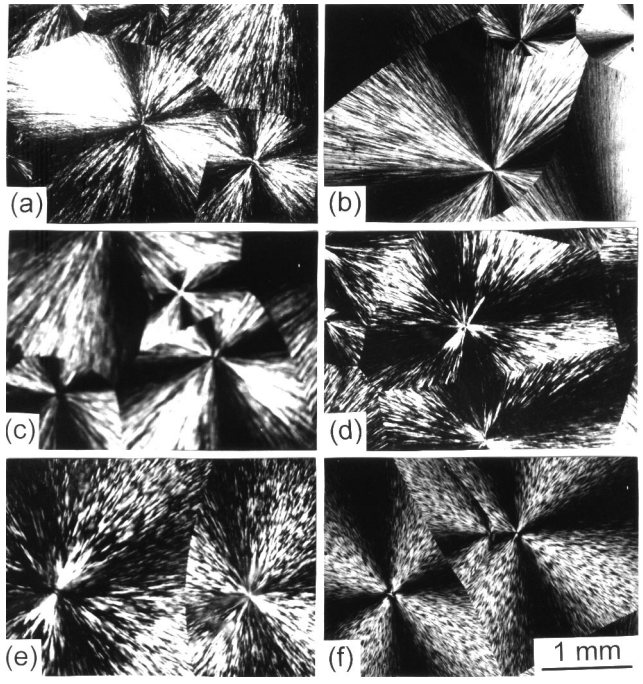


Fig. 12. Optical micrographs of ER/PEO blends crystallized at 23°C. ER/PEO: (a) 0/100; (b) 10/90; (c) 20/80; (d) 30/70; (e) 40/60; and (f) 50/50.

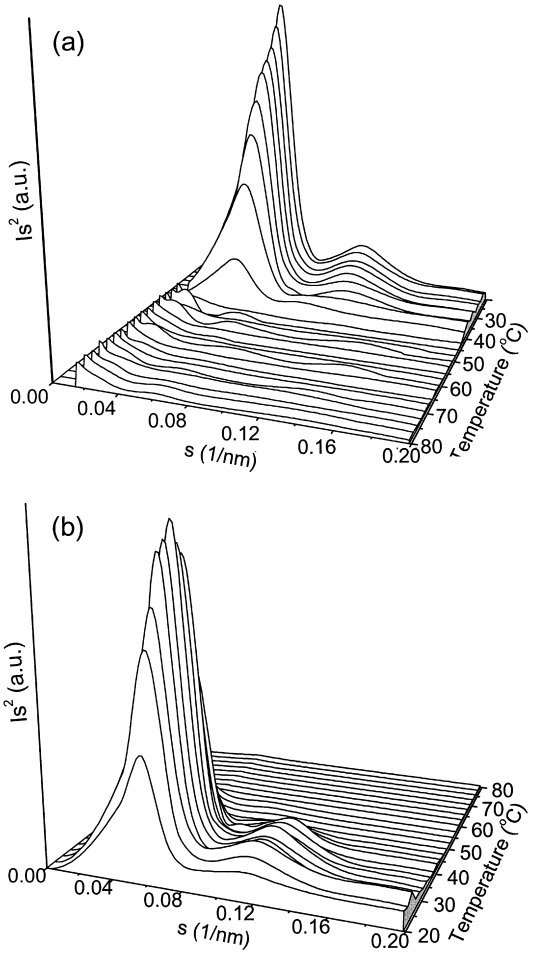


Fig. 13. Lorentz corrected SAXS patterns of a 10/90 ER/PEO blend during (a) cooling at 10°C/min from 80 to 20°C and (b) heating at 10°C/min after cooling. The experimental data have been smoothed using splines ($s = 2 \sin\theta/\lambda$, $2\theta$ is the scattering angle and $\lambda$ the wavelength = 0.15 nm).

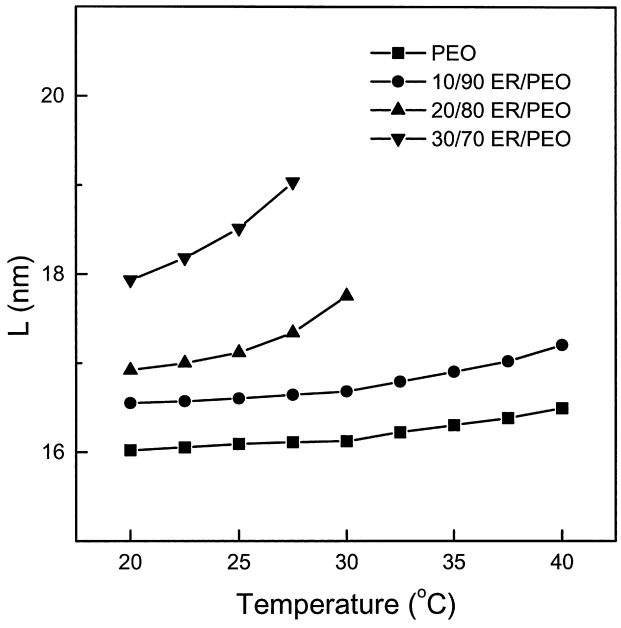


Fig. 14. Variation of the long period $L$ vs. temperature for MCDEA-cured ER/PEO blends during cooling at −10°C/min from 80 to 20°C.

following expression is obtained

$$f(K_n) \equiv \frac{1}{n}\ln K_n - \ln v_2 + \frac{C_1}{R(C_2 + T_c - T_g)} - \frac{0.2T_m^{eq}\ln v_2}{\Delta T} = \ln A_0 - \frac{K_g}{fT_c\Delta T} \quad (13)$$

The plots of $f(K_n)$ vs. $1/(fT_c\Delta T)$ for PEO and for the ER/PEO blends are shown in Fig. 10. The experimental data are linear. The values of $K_g$ and $A_0$ obtained from the slopes and the intercepts of the lines are listed in Table 3. Using Eq. (10), the $K_g$ values can further be used to evaluate $\sigma_e$ for all compositions and these values are also summarized in Table 3. The following parameters are used in the calculation: $\sigma = 0.1b_0\Delta H_f$, $Z = 4$, $b_0 = 4.65\times10^{-8}$cm, $R = 1.987$ cal/(mol K) and $k_B = 1.380\times10^{-23}$J/K.

In Fig. 11, the values of $\sigma_e$ and $A_0$ are plotted vs. composition. The value of $\sigma_e = 6.25\times10^{-2}$ J/m$^2$ for PEO is comparable with that obtained by Dubini et al. [39] ($6.0\times10^{-2}$ J/m$^2$) and by Cimmino et al. [40] ($7.5\times10^{-2}$ J/m$^2$). As illustrated in Fig. 11, the curve of $\sigma_e$ vs. composition for the cured blends exhibits a minimum. This result can be accounted for by combination of the surface enthalpy and entropy of folding ($\sigma_e = H_e - TS_e$) [41]. The initial decrease of $\sigma_e$ value with increasing ER content up to 20 wt% should be ascribed to the fact that the variation of the entropic term dominates that of the enthalpic one. The unfavorable enthalpic term is no longer negligible when the ER content in the ER/PEO blends reaches 30 wt%. The pre-exponential factor $A_0$ also depends on the composition and has a maximum in the vicinity of 10/90 ER/PEO.

### 3.4. Segregation phenomena and real-time SAXS investigation of the semicrystalline morphology

Crystallization in a miscible blend involves diffusion of the crystallizable component towards the crystallization front and rejection of the non-crystallizable component. The liquid–solid phase separation occurring during the crystallization process of PEO in miscible MCDEA-cured ER/PEO blends requires the segregation and diffusion of amorphous cured ER away from the crystalline nucleus. The cured ER molecules have a rather limited mobility compared to the linear polymer diluents.

PEO spherulites were observed in the cured ER/PEO blends with ER content up to 50 wt%. Fig. 12 shows the optical micrographs of these blends isothermally crystallized at 23°C. The blends with PEO content down to 50 wt% are still completely volume-filled with spherulites, and the size of the spherulites does not decrease with increasing ER content. The spherulitic morphology does not become more irregular or coarser. This implies that there is no interspherulitic segregation of MCDEA-cured ER. Consequently, the amorphous cured ER molecules must be segregated interlamellarly or interfibrillarly during the crystallization process of PEO.

Real-time SAXS measurements have been performed for samples of plain PEO and 10/90, 20/80, 30/70 MCDEA-cured ER/PEO blends. Fig. 13 shows Lorentz-corrected and smoothed real-time SAXS patterns of a 10/90 cured ER/PEO blend during cooling from 80 to 20°C at 10°C/min (Fig. 13(a)) and during the subsequent heating

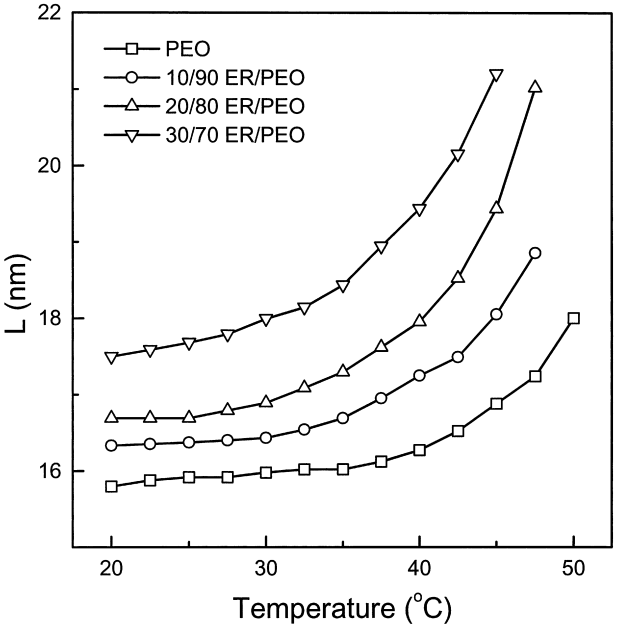


Fig. 15. Variation of the long period $L$ vs. temperature for MCDEA-cured ER/PEO blends during heating at 10°C/min from 20 to 80°C.

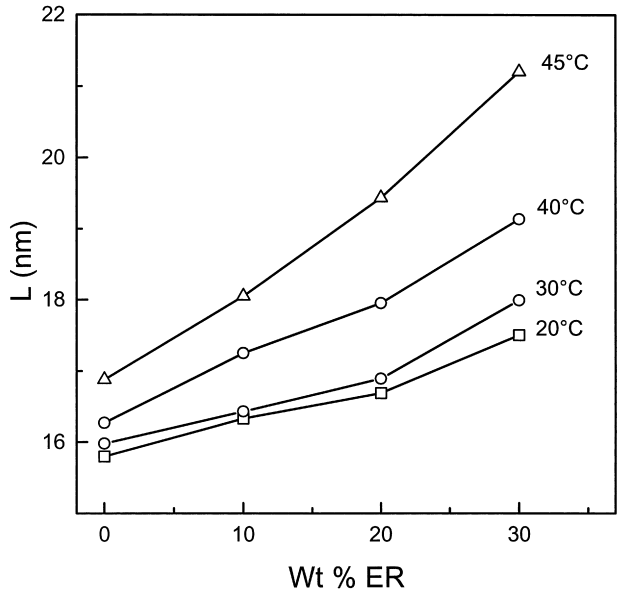


Fig. 16. Long period $L$ as a function of composition for MCDEA-cured ER/PEO blends during heating at 10°C/min from 20 to 80°C.

from 20 to 80°C at 10°C/min (Fig. 13(b)). Fig. 13(a) illustrates that a maximum of scattering intensity appears at low temperatures during cooling, indicating the formation of crystalline lamellae of PEO in the blend. During the subsequent heating as shown in Fig. 13(b), the maximum of scattering intensity first increases, implying that the crystallization was not complete during the cooling process. The maximum subsequently decreases and finally disappears at high temperatures. Similar real-time SAXS patterns were also obtained for pure PEO and for 20/80 and 30/70 cured ER/PEO blends.

The long period $L$ can be evaluated from the maximum of Lorentz-corrected SAXS patterns. Fig. 14 displays the evaluation of the long period $L$ as a function of temperature for the pure PEO and the three blends during the cooling scans. For pure PEO and the 10/90 ER/PEO blend, a maximum in the Lorentz-corrected real-time SAXS patterns appears at 40°C during cooling. For the 20/80 and 30/70 ER/PEO blends, the maximum appears at lower temperatures. The incorporation of ER component hinders the crystallization of PEO. As illustrated in Fig. 14 the long period $L$ decreases with decreasing temperature during cooling for pure PEO as well as for the three blends. Moreover, at a given temperature the long period $L$ increases with increasing ER content.

Fig. 15 illustrates the variation of long period $L$ with temperature for pure PEO and for the blends during the subsequent heating after the cooling from the melt. The long period $L$ increases with increasing temperature in all cases. The increase in long period $L$ upon heating can be ascribed to the progressive melting of the less stable crystalline lamellae and subsequent recrystallization; such a melting-recrystallization mechanism results in an increase of the long period.

Fig. 16 represents the long period $L$ as a function of blend composition at different temperatures. The long period $L$ increases drastically with increasing ER content at all temperatures, suggesting that interlamellar segregation occurs in the cured ER/PEO blends. Interlamellar segregation of the amorphous diluent between the crystalline lamellae will result in an increase of the long period $L$ as shown in a number of cases for miscible polymer blends [42–46], e.g. poly(vinyl chloride) with poly(ϵ-caprolactone) (PCL) [42] and poly(styrene-*co*-maleic anhydride) with PCL [43]. In contrast, interfribrillar segregation has no influence on the thickness of the amophous between the crystalline lamellae and hence on the long period $L$. This type of segregation has been reported for isotactic polystyrene/atactic polystyrene blends [47]. It is clear that, in the present ER/PEO blends, the amorphous cured ER molecules segregated interlamellarly during the crystallization process of PEO.

The occurrence of interlamellar segregation in the cured ER/PEO blend can be fully understood if one considers the low chain mobility of the cured ER in the ER/PEO blends. The cured ER molecules diffuse slowly away from the crystal growth nucleus compared to a conventionally linear diluent polymer in a miscible non-crystalline/crystalline blend. The low chain flexibility and high $T_g$ of the cured ER could be responsible for the hindered diffusion. It is still difficult to imagine the segregation process of the ER network in the blend during the crystallization of PEO. The ER network should have a strong topological influence on

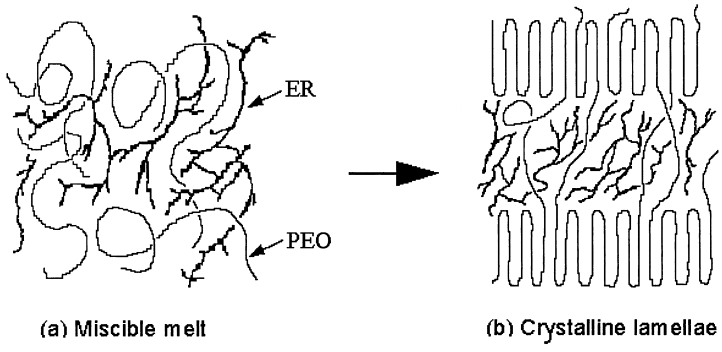


Fig. 17. Model describing (a) the miscible melt and (b) the crystalline lamellae of the MCDEA-cured ER/PEO blends.

the crystallization and segregation. It should be pointed out that, for the blends with PEO content as high as 70 wt% or more, the curing reaction could hardly be completed. In order to avoid thermal degradation of PEO, the curing temperatures used in this study were, however, not sufficiently high and the ER was actually not sufficiently cured in the blends with 70 wt% PEO or higher. Generally, curing reaction involves chain extension, branching and crosslinking. As the curing reaction proceeds, the molecular weight of the system rapidly increases. The crosslink density of the ER network in the ER/PEO blends should be crucially dependent on the blend composition. For the blends with low PEO content, a three-dimensional crosslinking network structure forms; the blends display a homogeneous semi-interpenetrating network (semi-IPN) structure. In this semi-IPN, the initially miscible components still exhibit characteristic features of miscibility because of favorable hydrogen-bonding interactions. In contrast, for the blends with low ER content, there are only highly branched chain molecules and an imperfect network is formed. This type of cured ER molecules has a very limited mobility and can only very slowly diffuse away from the crystallization front.

Fig. 17 schematically illustrates a model of the structure of a cured ER/PEO blend in the miscible melt and the lamellar structure in the crystallized blend. In the melt, PEO is miscible with the highly branched ER molecules and the imperfect ER network, and the blend has a homogeneous structure. In the crystallized blend, the semicrystalline morphology is a stack of crystalline lamellae; the amorphous fraction of PEO, the branched ER chains and imperfect ER network are located between PEO lamellae. The highly branched ER chains and the imperfect ER network are segregated interlamellarly during the crystallization process of PEO in the MCDEA-cured ER/PEO blends.

## 4. Conclusions

MCDEA-cured ER/PEO blends are completely miscible over the entire composition range. Both the overall crystallization rate and crystallinity of PEO in the cured ER/PEO blends decrease with increasing ER content. The incorporation of the MCDEA-cured ER lowers the molecular mobility and has strongly hindders crystallization of PEO in the ER/PEO blends. There is hydrogen-bonding between the hydroxyl groups of MCDEA-cured ER and the ether oxygens of PEO in the cured system, which is responsible for the miscibility in the cured blends. The average strength of the hydrogen bond in the cured ER/PEO blends is higher than that in the pure cured ER. The crystallization behavior of PEO from the melt is strongly influenced by the composition and the crystallization temperature. At high conversion, the time dependence of the relative degree of crystallinity deviates from the Avrami equation. Addition of a non-crystallizable ER component into PEO causes a depression of both the overall crystallization rate and the melting temperature. The surface free energy of folding $\sigma_e$ displays a minimum when the composition is varied. The crystalline morphology of PEO in the cured ER/PEO blends displays typical characteristics of miscible/crystalline blends, and the PEO spherulites are always completely volume-filling. The semicrystalline morphology is a stack of crystalline lamellae and the long period $L$ increases drastically with increasing ER content at a given temperatures. The highly branched ER chains and the imperfect ER network are segregated interlamellarly during the crystallization of PEO. Interlamellar segregation in the cured ER/PEO blend can be considered to be due to the low chain mobility of the cured ER in the ER/PEO blends.

## Acknowledgements

The authors are indebted to Dr F. Defoor, Shell Research, Louvain-la-Neuve, Belgium, for kindly supplying the Epikote 828EL sample and to the Fund for Scientific Research Flanders (F.W.O.-Vlaanderen) for financial support to the MSC lab. One of us (Q.G.) wishes to express his appreciation to the KU Leuven Research Council for awarding a Senior Fellowship for Visiting Professors.

## References

[1] Guo Q. In: Shonaike GO, Simon G, editors. Polymer blends and alloys. New York: Marcel Dekker, 1999. p. 155–87 (chap. 6).
[2] Noshay A, Robeson LM. J Polym Sci, Polym Chem Ed 1974;12:689.
[3] Clark JN, Daly JH, Garton A. J Appl Polym Sci 1984;9:3381.
[4] Guo Q, Peng X, Wang Z. Polym Bull 1989;21:593.
[5] Mucha M. Colloid Polym Sci 1994;272:1090.
[6] Zheng H, Zheng S, Guo Q. J Polym Sci, Polym Chem Ed 1997;35:3161.
[7] Zheng H, Zheng S, Guo Q. J Polym Sci, Polym Chem Ed 1997;35:3169.
[8] Zhong Z, Guo Q. Polymer 1998;39:517.
[9] Luo X, Zheng S, Zhang N, Ma D. Polymer 1994;35:2619.
[10] Zheng S, Zhang N, Luo X, Ma D. Polymer 1995;36:3609.
[11] Guo Q, Peng X, Wang Z. Polymer 1991;32:53.
[12] Horng TJ, Woo EM. Polymer 1998;39:4115.
[13] Koch MHJ, Bordas J. Nucl Instrum Methods 1983;208:461.
[14] Boulin CJ, Kempf R, Koch MHJ, McLaughlin SM. Nucl Instrum Methods A 1986;249:399.
[15] Vidotto G, Levy DL, Kovacs AJ. Kolloid Z Polym 1969;230:289.
[16] Gordon M, Taylor JS. J Appl Chem 1952;2:495.
[17] Fernandes AC, Barlow JW, Paul DR. J Appl Polym Sci 1984;29:3381.
[18] Wunderlich B. Macromolecular physics, vol. 2. New York: Academic Press, 1976 (p. 24).
[19] Nishi T, Wang TT. Macromolecules 1975;8:909.
[20] Imken RL, Paul DR, Barlow JW. Polym Engng Sci 1976;16:593.
[21] Defieuw G, Groeninckx G, Reynaers H. Polymer 1989;30:595.
[22] Robeson LM, Hale WF, Merriam CN. Macromolecules 1981;14:1644.
[23] Coleman MM, Moskala EJ. Polymer 1983;24:251.
[24] Purcell KF, Drago RS. J Am Chem Soc 1968;89:2874.
[25] Avrami M. J Chem Phys 1962;37:1723.

[26] Schultz JM. Polymeric materials science. New York: Prentice Hall, 1981.
[27] Ong CJ, Price FP. J Polym Sci, Polym Symp 1978;63:45;59.
[28] Wunderlich B. Macromolecular physics, vol. 2. New York: Academic Press, 1976 (p. 146).
[29] Grenier D, Prud'homme ER. J Polym Sci, Polym Phys Ed 1980;18:1655.
[30] Hoffman JD, Weeks JJ. J Chem Phys 1962;37:1723.
[31] Hoffman JD, Weeks JJ. J Res Natl Bur Stand, Sect A 1962;66:13.
[32] Hoffman JD. Soc Plast Engng Trans 1960;4:315.
[33] Hoffman JD, Frolen LJ, Ross GS, Lauritzen JI. J Res Natl Stand, US 1975;79A:671.
[34] Hoffman JD. Polymer 1983;24:3.
[35] Boon J, Azcue JM. J Polym Sci A-2 1968;6:885.
[36] Clark EJ, Hoffman JD. Macromolecules 1984;17:878.
[37] Williams ML, Landel RF, Ferry JD. J Am Chem Soc 1955;77:3701.
[38] Hoffman JD, Davis GT, Lauritzen JI. In: Hannay NB, editor. Treatise on solid state chemistry, vol. III. New York: Plenum Press, 1976 (chap. 7).
[39] Dubini PE, Beltrame PL, Canetti M, Seves A, Marcandalli B, Martuscelli E. Polymer 1993;34:996.
[40] Cimmino S, Martuscelli E, Silvestre C, Canetti M, Delalla C, Seves A. J Polym Sci, Polym Phys Ed 1989;27:1781.
[41] Martuscelli E, Pracella M, Yue WP. Polymer 1984;25:1097.
[42] Khambatta FH, Warner FP, Russell TP, Stein RS. J Polym Sci-A2 1976;14:1391.
[43] Defieuw G, Groeninckx G, Reynaers H. Polymer 1989;30:2158.
[44] Dreezen G, Koch MHJ, Reynaers H, Groeninckx G. Polymer 1999;40:6451.
[45] Dreezen G, Mischenko N, Koch MHJ, Reynaers H, Groeninckx G. Macromolecules 1999;32:4015.
[46] Guo Q, Harrats C, Groeninckx G, Reynaers H, Koch MHJ. Submitted for publication.
[47] Warner FP, MacKnight WJ, Stein RS. J Polym Sci, Polym Phys Ed 1977;15:2113.